28th AIAA/CEAS Aeroacoustics 2022 Conference, 14-17 June 2022, Southampton, UK.
DOI: 10.2514/6.2022-2909

LES study of noise and its sources of closely installed jets

Zhong-Nan Wang[1]
University of Birmingham, Birmingham, England B15 2TT, UK
University of Cambridge, Cambridge, England CB2 1PZ, UK

Anderson Proenca[2]
Cranfield University, Cranfield, England MK43 0AL
University of Southampton, Southampton, England SO17 1BJ, UK

Jack Lawrence[3]
University of Southampton, Southampton, England SO17 1BJ, UK

Paul Tucker[4]
University of Cambridge, Cambridge, England CB2 1PZ, UK

Rod Self[5]
University of Southampton, Southampton, England SO17 1BJ, UK

When a jet is closely installed under a solid surface, the turbulent jet plume is modified. Two levels of jet-plate interactions are present. In addition to linear evanescent instability wave scattered by the plate trailing edge, nonlinear jet turbulence strongly interacts with the plate underneath. Both of the interactions could lead to far-field noise change but with different mechanisms. Large-Eddy Simulation (LES) has been performed on two installed jets and one baseline isolated jet to investigate the noise generation mechanisms for this closely installed jet. The distance between jet and plate surface is adjusted for the two installed jets so that strong hydrodynamic interaction is only present in one of the configurations. Far-field noise, computed using Ffowcs Williams-Hawkings (FW-H) equations, is compared for the two installed jets to show the effect of close installation. The near-field sound sources are examined by analysing quadrupole sources of turbulent mixing and dipole sources of unsteady plate surface loading.

Nomenclature

D	=	nozzle diameter
H	=	vertical distance between the jet centre line and the plate underneath
L	=	axial distance between jet exit and plate trailing edge
W	=	half-width of the flat plate
U	=	time-averaged velocity
$\boldsymbol{u}$	=	velocity fluctuations (u_1, u_2, u_3)
M	=	Mach number
(x,y,z)	=	Cartesian coordinates
(x,r,θ)	=	cylindrical coordinates, *i.e.* axial, radial and azimuthal coordinates

[1] Lecturer (Assistant Professor), College of Engineering and Physical Sciences, University of Birmingham; Visiting Scholar, Deparment of Engineering, University of Cambridge. Member AIAA.
[2] Reserach Fellow in Experimental Aerodynamics, Applied Aerodynamic Group, Cranfield University; Visiting Fellow, Acoustics Group, University of Southampton. Member AIAA.
[3] Research Fellow, Institue of Sound and Vibration Research. Member AIAA.
[4] Rank Professor of Engineering, Department of Engineering. Associate Fellow AIAA.
[5] Professor of Aeroacoutics, Institue of Sound and Vibration Research. Member AIAA.

Published by AIAA. This is the Author Accepted Manuscript issued with: Creative Commons Attribution Non-Commercial License (CC:BY:NC 4.0).
The final published version (version of record) is available online at DOI:10.2514/6.2022-2909. Please refer to any applicable publisher terms of use.

Script

rms = root square mean
j = jet exit

I. Introduction

AIRCRAF noise is a major concern to communities neighbouring airports [1]. Jet noise from aeroengines is still the dominant component when an aircraft is taking off. High-bypass-ratio engines reduce jet noise by lowering the jet exit speed. However, when the bypass ratio is increased, the jet engine is installed closer to the wing. This significantly intensifies jet noise due to the strong interaction between the jet and wing. This is normally referred to as installed jet noise and usually occurs in the low-frequency range. Historically, the extra noise due to the wing installation was first noticed by Bushell [2] by comparing the in-flight installed jet with a static isolated jet for a full-scale aircraft. The characteristics of this installed jet have been studied vastly by experimentalists [3-5]. The directivity of installation noise is found to be dipole-like and it is also sensitive to the distance from the jet to the solid surface and the distance from the jet exit to the surface trailing edge. To understand the mechanism, Ffowcs William and Hall in 1970 observed that the far-field low-frequency noise can be amplified when a turbulent flow is next to a surface [6]. They attributed this amplification to the hydrodynamic scattering near the solid surface edge. Lyu and Dowling confirmed this theory and developed a reliable prediction model [7] based on hydrodynamic wave scattering. It demonstrated that the far-field sound amplification can be accurately predicted by incorporating the scattering of the near-field hydrodynamic evanescent wave using the Amiet approach [8]. It should be noted that this prediction method is valid for the solid surface sitting in the irrotational flow region, therefore regarded as a linear mechanism of noise amplification for installed jets. However, when the solid surface moves close to the surface, such as in Ultra-High Bypass-Ratio engine installation, the nonlinear interaction between the jet and solid surface begins to increase. The jet mixing shear layer near the solid surface is significantly altered. The jet mixing noise source is likely to be modified in a closely-installed configuration [9]. This could further result in far-field noise change at relatively high frequencies. There is still a lack of consensus in understanding this scenario, which puts the noise generation mechanism of installed jets incomplete for realistic applications.

In this paper, we will use Large Eddy Simulation (LES) to investigate the interactions and their generated noise in closely installed jets. The comparisons of near-field flows and far-field noise are made between the two installed jets with different distances between the jet and the plate. Two noise sources, i.e. quadrupole sources of turbulent mixing in the jet plume and dipole sources of unsteady loading on the plate, are examined to evaluate the impact of the close installation.

II. Case Description

To investigate the installation effects on jet noise, canonical cases are first designed to model installation conditions. A single stream jet is placed under a flat plate, shown in Figure 1. The jet operates at Mach number 0.6, which is representative of UHBPR engines. Two parameters are used to control the position of the jet relative to the flat plate. *H* represents the vertical distance from jet centreline to plate surface and *L* represents the distance from jet exit to plate trailing edge.

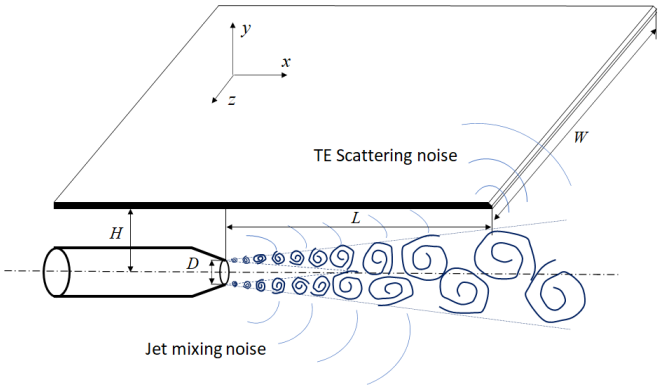


Figure 1 Schematic of canonical installed jets

The installation configurations of three cases are listed in Table 1. For installed case 1, the jet flow creeps past the plate trailing edge without touching it; for installed case 2, the plate is wetted by the jet shear layer, where more nonlinear hydrodynamic interactions are expected. The experimental measurements have already been performed on these installed configurations using hot wires [10].

Table 1 Jet installation configurations

Case name	M_j	L/D	H/D
Iso	0.6	-	-
H100	0.6	4.00	1.00
H067	0.6	4.00	0.67

III. Numerical methods

A. Near-field flow simulation

LES requires a numerical scheme with low dissipation characteristics to resolve approximately 90 percent of flow energy. A non-dissipative numerical scheme is developed using the kinetic energy preserving (KEP) property[11] to ensure the computation is stable without any artificial dissipation. The scheme is blended with 4th order Laplacian smoothing and gradually stretching grids towards the computational boundary to be non-reflective. As to the turbulence modelling, a RANS layer is included near the wall to model the boundary layer on the nozzle. The RANS layer is blended with the LES region using a specially designed blending function based on modified wall distance[12, 13]. In this simulation, the SA RANS model[14] and the WALE SGS model [15] are used to treat the turbulence in different regions.

B. Far-field acoustic prediction

To predict the far-field acoustics, FW-H integration is performed over time series of flow data on the near-field FW-H surfaces. Three FW-H surfaces are placed with increased radial positions around the jet plume and plate. This is to ensure the surfaces lie in the irrotational region and enclose all the quadruple sources so that a robust and accurate far-field sound prediction can be obtained. The detail of the near-field FW-H surface placement can be found in our previous publication [16]. The far-field noise prediction is also made by placing the FW-H surface on the plate to evaluate the noise generation from the unsteady surface loading, caused by the jet-plate interaction.

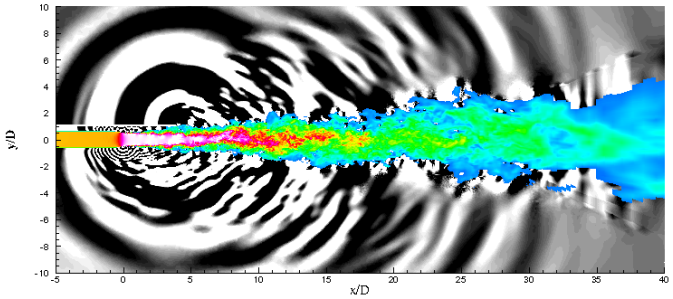
The flow simulation method and the FW-H approach used here have been fully validated using the isolated and the first installed cases [16]. The near-field statistics and spectra are compared with hot-wire measurements and the far-field noise has been validated with microphone data. This paper is primarily focused on the second installation case, as the jet plume is altered by the plate.

IV. Results and Discussions

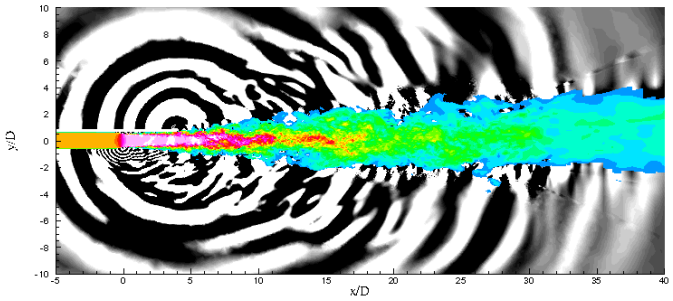
A. Overview of flow fields

For the flow fields, the first installed jet with H/D=1 slightly scrapes the plate trailing edge without significant modification of flow structures, while the second jet, with closer installation H/D=0.67, touches the underneath of the plat plate, leading to nonlinear hydrodynamic interactions. These interactions will modify the upper jet shear layer. This jet plume modification by the plate is expected to have an impact on mixing noise sources and will be shown in detail in subsection D. As to the acoustics, a new sound source is introduced around the trailing edge (TE) in addition to the jet mixing noise. The Figure 1 schematic has been used to illustrate this new source. This new source is present in both installed jets. It is generated by scattering near-field evanescent hydrodynamic waves into propagating acoustics. The scattering sources are linked with dipole sources on the plate, which will be examined later.

For H/D=1, the jet just scratches the plate trailing edge and the jet plume is not altered by the plate. The installation noise primarily comes from the scatterings from near-field instability waves. However, for H/D=0.67, the jet wets the plate underneath, inducing strong hydrodynamic interactions. This leads to a modification of the jet plume and could further lead to an additional change of far-field noise in addition to the increase of instability wave scattering at the plate trailing edge.



(a) installed jet with *H/D*=1.0



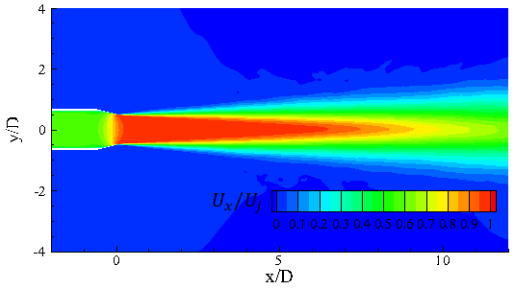
(b) installed jet with *H/D*=0.67

Figure 2 Flow and acoustics of two installed jets: axial velocity in colour contours and pressure time derivatives in grey-scale contours

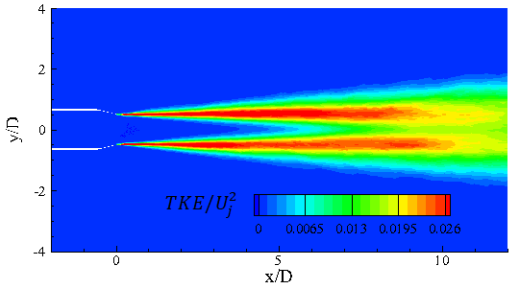
B. Time-averaged flows

The time-averaged flows and the turbulent kinetic energy (TKE) are shown in Figure 3. The installed jet with *H/D*=1 remains almost the same as the isolated jet, as seen in Figure 3 (c) and (d). The jet flow creeps past the flat plate tailing edge. The jet plume does not look affected by the presence of a flat plate. Therefore, this is a good case for studying the instability wave scattering with no jet noise source modification. Nonlinear interactions are evident in the installed jet with H/D=0.67 as the jet upper shear layer spreading is significantly restricted by the plate, as seen in Figure 3 (e). The jet shear layer scratches the underneath surface of a flat plate. As a result of the blockage introduced by the plate, turbulence is reduced near the solid surface, shown in Figure 3, and the jet plume is squashed in the radial direction under the plate, which consequently changes the quadruple noise source distribution.

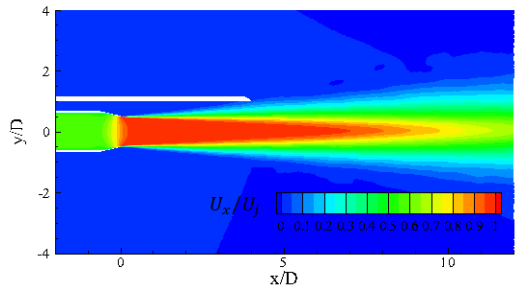
Figure 4 shows the radial profiles of mean velocities and their fluctuations downstream of the jet nozzle exits. The LES prediction agrees well with the hot-wire measurement. The validation was also performed in near-field velocity and pressure spectra as well as space-time velocity correlations. More validation detail can be found in our previous publication [16]. The jet flow is restricted under the plate at *H/D*=0.67. In the upper shear layer, the flow accelerates under the plate with decreased TKE. However, directly downstream of the plate, the TKE of installed jet *H/D*=0.67 grows larger than that of the other two cases, due to the strong interaction between the jet and plate. Further downstream, the jet flow recovers to a similar state of the isolated jet at *x/D*=8, 4*D* downstream of the plate trailing edge.



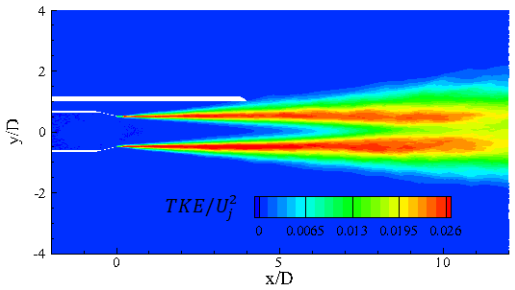
(a) Axial velocity in the isolated jet



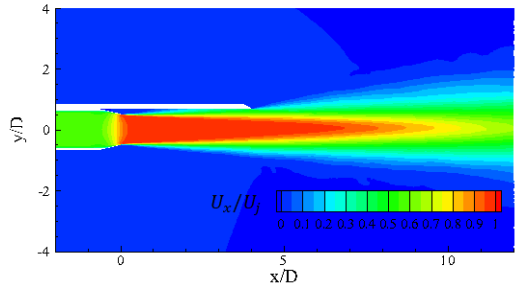
(b) Turbulent kinetic energy in the isolated jet



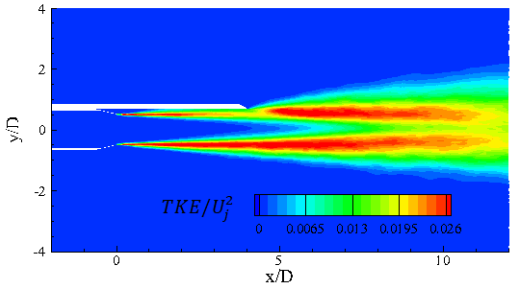
(c) Axial velocity in the installed jet (*H/D*=1)



(d) Turbulent kinetic energy in the isolated jet (*H/D*=1)

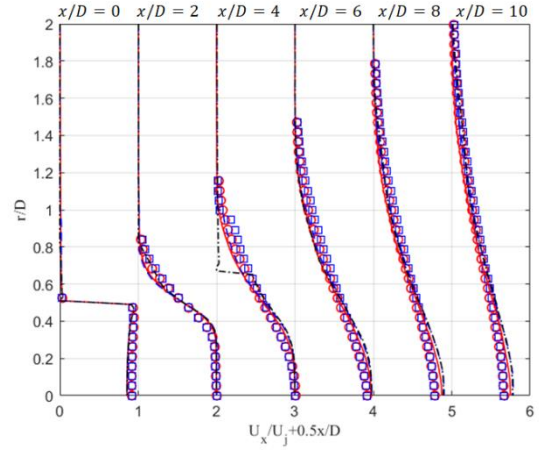


(e) Axial velocity in the installed jet (*H/D*=0.67)

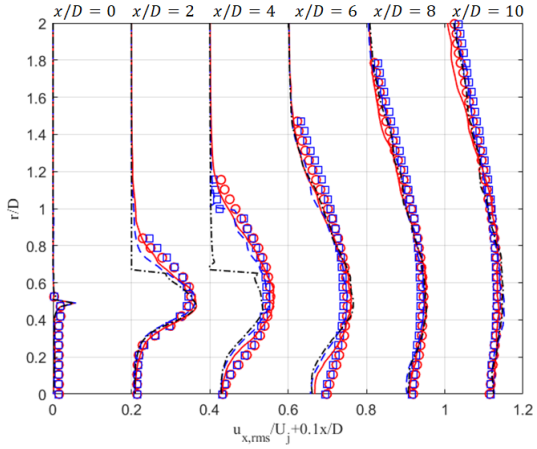


(f) Turbulent kinetic energy in the isolated jet (*H/D*=0.67)

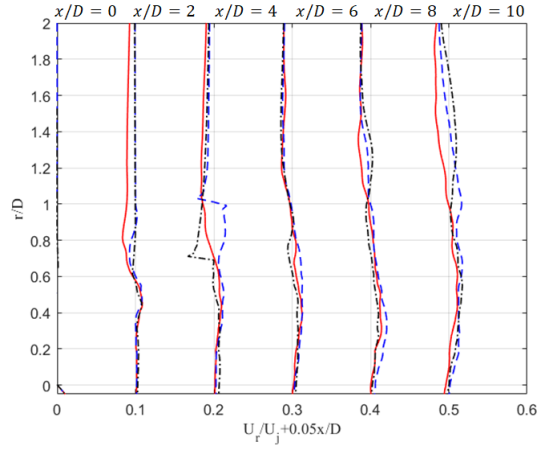
Figure 3 Time-averaged velocity and turbulent kinetic energy (TKE) for isolated and installed jets at the plane of *z*=0



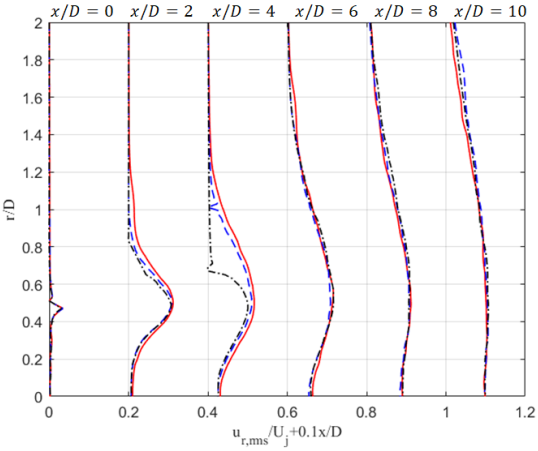
(a) axial velocity



(b) axial velocity fluctuations



(c) radial velocity

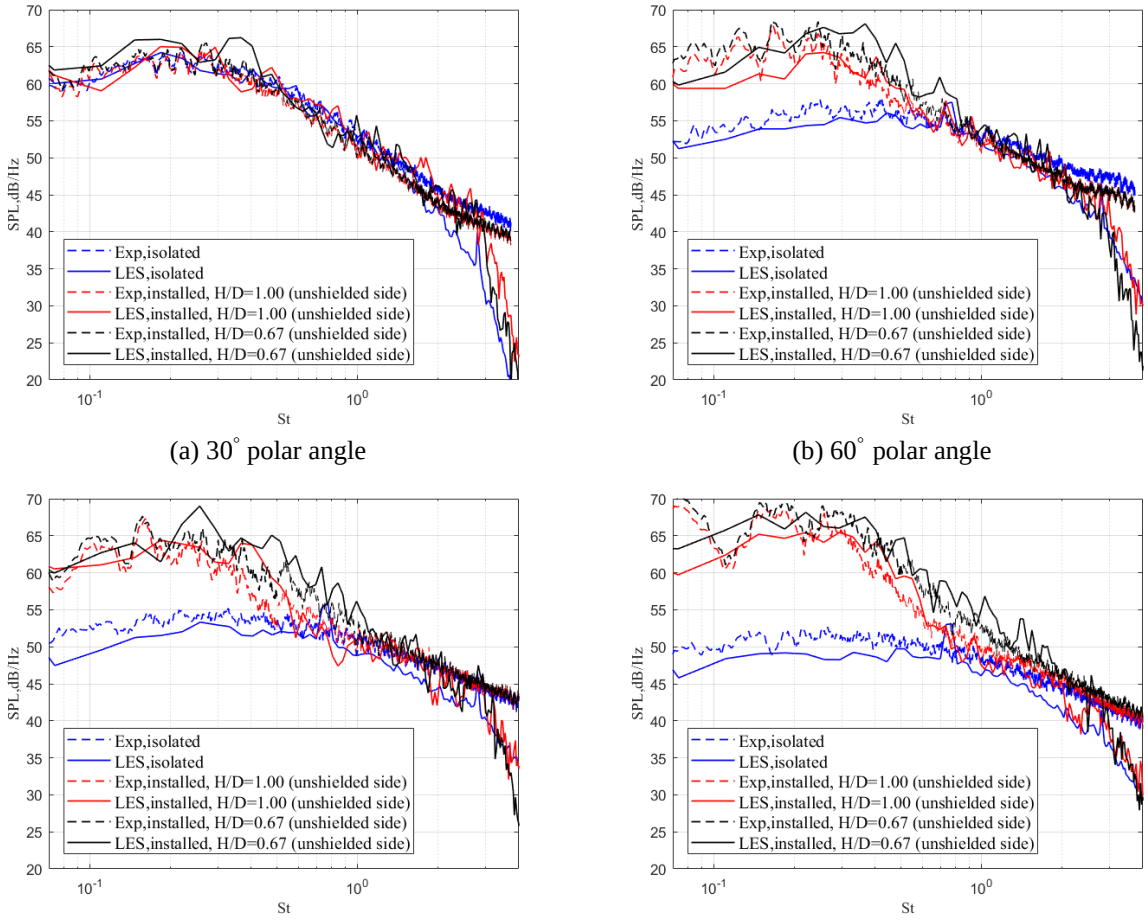


(d) radial velocity fluctuations

Figure 4 Radial profiles of time-averaged axial and radial velocities and the fluctuations around them at various axial locations: dots represent experimental measurements, while lines represent LES prediction; the isolated jet is plotted in red, the installed jets with H/D=1 in blue and the installed jet with H/D=0.67 in black.

C. Far-field noise

Figure 5 shows the far-field noise of the isolated and installed jets at four polar angles. The polar angle is defined as the angle between the observer vector and the jet flow direction. The far-field noise at the unshielded side is shown for the installed jets. The unshielded side refers to the side below the plate as shown in Figure 1. The far-field noise is measured at a different Mach number, i.e. M_j=0.5, instead of M_j=0.6, so the noise is scaled to the M_j =0.6. The predictions are in a reasonably good agreement with the trend of microphone measurement. At the downstream polar angle 30°, the installed jet noise remains close to the isolated jet noise. As the polar angle increases, the installed noise increases in the frequency range below St=1. This agrees with the feature of a dipole noise source. For the closely-coupled jet configuration *H/D*=0.67, the noise increase and its amplified frequency range are larger than those of the installed jet with *H/D*=1. We will investigate in the next section what causes this far-field noise change between the installed jet of H/D=0.67 and 1 from the perspectives of noise sources.



(a) 30° polar angle (b) 60° polar angle

(c) 90° polar angle (d) 120° polar angle

Figure 5 Far-field noise with four polar angles (30°, 60°, 90° and 120°) from the downstream direction on the unshielded side

D. Noise source analysis

In the framework of acoustics analogy, installed jet noise is generated by two major noise sources: quadrupole sources of turbulent mixing in the jet plume and dipole sources of unsteady forces exerted on the plate. As the plate is

stationary, displacement-induced monopole sources are absent in this case. In this section, we will examine the change in the quadrupole and dipole sources when the plate is moved closer to the jet.

1. Quadrupole sources

In the Goldstein acoustics analogy [17, 18], far-field jet noise can be obtained by convoluting the quadrupole sources, characterised by 4th order space-time correlation of velocities, with a Green's function over the jet plume. The 4th order velocity correlation $R_{ijkl}(\boldsymbol{x};\delta\boldsymbol{x},\tau)$ can be informed using LES data and used here to characterise the sources of jet mixing noise. It is calculated by correlating the 2nd order velocity stress tensor $T_{ij}(\boldsymbol{x},t)$ at different spatial separation , $\delta\boldsymbol{x}$ and time delay τ, written as

$$R_{ijkl}(\boldsymbol{x};\delta\boldsymbol{x},\tau) = \overline{T_{ij}(\boldsymbol{x},t)T_{kl}(\boldsymbol{x}+\delta\boldsymbol{x},t+\tau)}$$

where $\boldsymbol{x}$ is the reference location which the spatial correlation is taken from. The velocity stress tensor $T_{ij} = -(\rho u_i'u_j' - \overline{\rho u_i'u_j'})$ has a zero time mean with overbears representing the time average. The velocity fluctuations $u_i' = u_i - \widetilde{u_i}$ is obtained based on Favre-averaged velocity $\widetilde{\boldsymbol{u}} = \overline{\rho\boldsymbol{u}}/\rho$.

The normalised 4th order velocity correlations $R_{1111}(\boldsymbol{x};\delta\boldsymbol{x},\tau)/R_{1111}(x;\boldsymbol{0},0)$ are plotted in Figure 6 on its reference centres $\boldsymbol{x}$ along the upper nozzle lipline $y/D = 0.5$ at the plane of $z/D = 0$ around the plate trailing edge at $x/D = 4$. Each correlation shows a peak in the centre and decays with the increase of spatial and temporal separations. Within certain spatial and temporal separations, the chaotic turbulence is statistically correlated and generates noise. For the installed jets, the effects of the plate are visible. As the plate is moved closer to the jet, the extent of the correlated region is changed. The extent of the correlated source region can be characterised by the integral length and time scales. These turbulence noise sources are not stationary, and they travel at a convective speed. The length and time scales of the sources need to be evaluated at a moving frame with the convection velocity, by integrating the normalised 4th order velocity correlations over space and time:

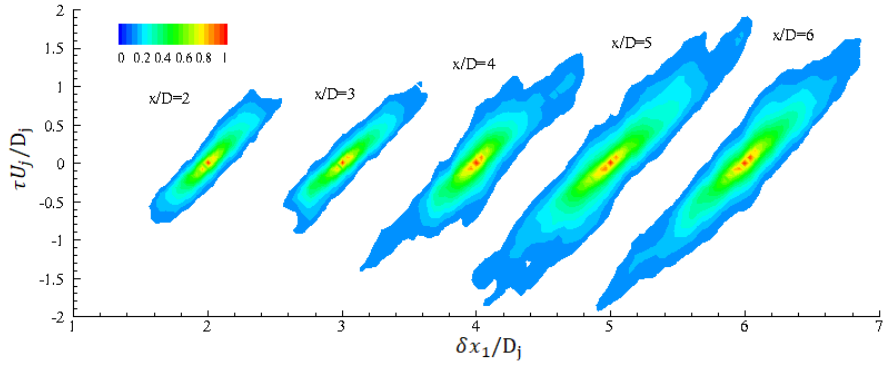
$$L_{ijkl}^{x_i}(\boldsymbol{x}) = \frac{1}{2}\int_{-\infty}^{+\infty}\frac{R_{ijkl}(\boldsymbol{x};\delta\boldsymbol{x},0)}{R_{ijkl}(x;\boldsymbol{0},0)}d\delta x_i$$

$$T_{c_i,ijkl}(\boldsymbol{x}) = \int_{0}^{+\infty}\frac{R_{ijkl}(\boldsymbol{x};\delta\boldsymbol{x}_{peak},\tau_{peak})}{R_{ijkl}(x;\boldsymbol{0},0)}d\tau_{peak}$$

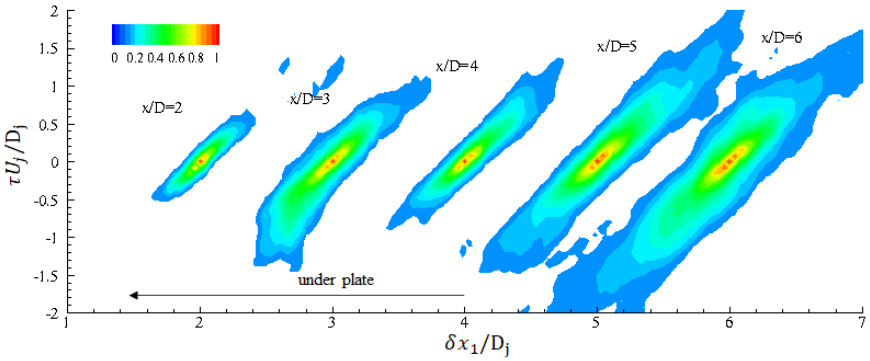
where $L_{ijkl}^{x_i}$ is the integral length scales of the correlation R_{ijkl} in the x_i direction, and $T_{c_i,ijkl}$ is the integral time scale of the correlation R_{ijkl} in the convection velocity in the x_i direction. The convection velocity $U_{c,ijkl}^{x_i}$ is obtained following the peak correlation location at each δx_i and τ:

$$U_{c,ijkl}^{x_i} = \delta x_{i,peak}/\tau_{peak}$$

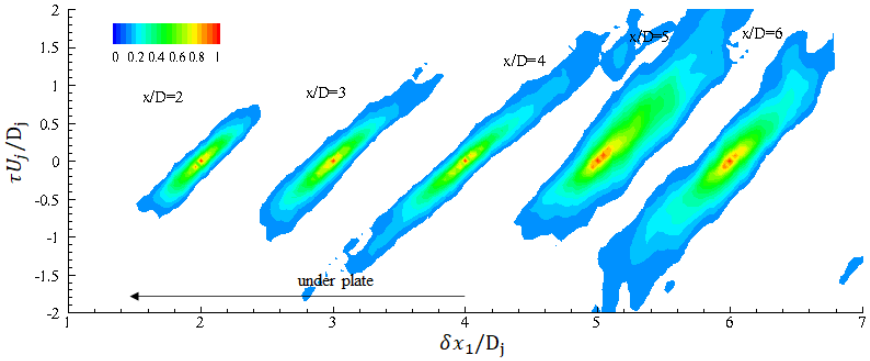
The integral time and length scales of the correlation R_{1111}in the axial direction is shown in Figure 7 (a) and (b). The time and length scales remain similar under the plate for the isolated and installed *H*/*D*=1.00. For the installed *H*/*D*=0.67, the plate restricts the turbulence development, so reducing the length scales, but the time scales seem not to be affected. Downstream of the plate, the installation shows the tendency to increase time and length scales. This increase becomes obvious in the close installation configuration *H*/*D*=0.67, as the jet flows have already interacted with the plate underneath and generated wake-like velocity profiles. A peak of length and time scales are evident between *x*=4*D* and 6*D*. This increase in source scales will potentially affect the mixing noise in the close installation case, *H*/*D*=0.67, as it changes the extent of the convolution of the sources with Green's function when obtaining the far-field sound. In addition, the close installation, *H*/*D*=0.67, also increases the convection velocity, shown in Figure 7 (c) as the flow is more accelerated under the plate compared to the installed case *H*/*D*=1.00.



(a) Isolated jet

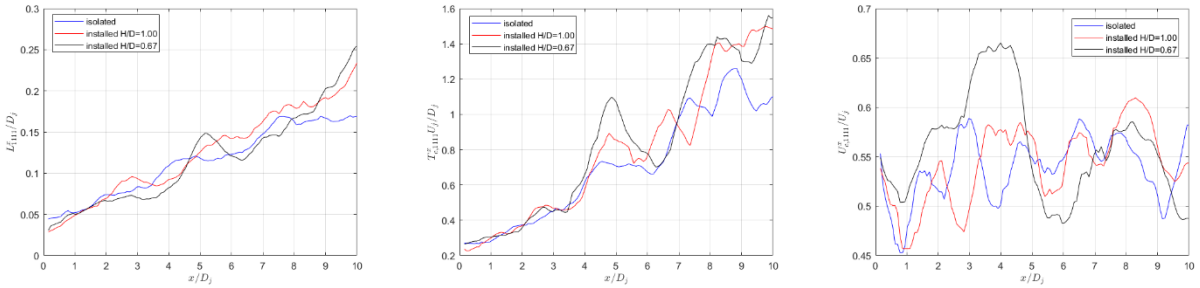


(b) Installed jet, H/D=1.00



(c) Installed jet, H/D=0.67

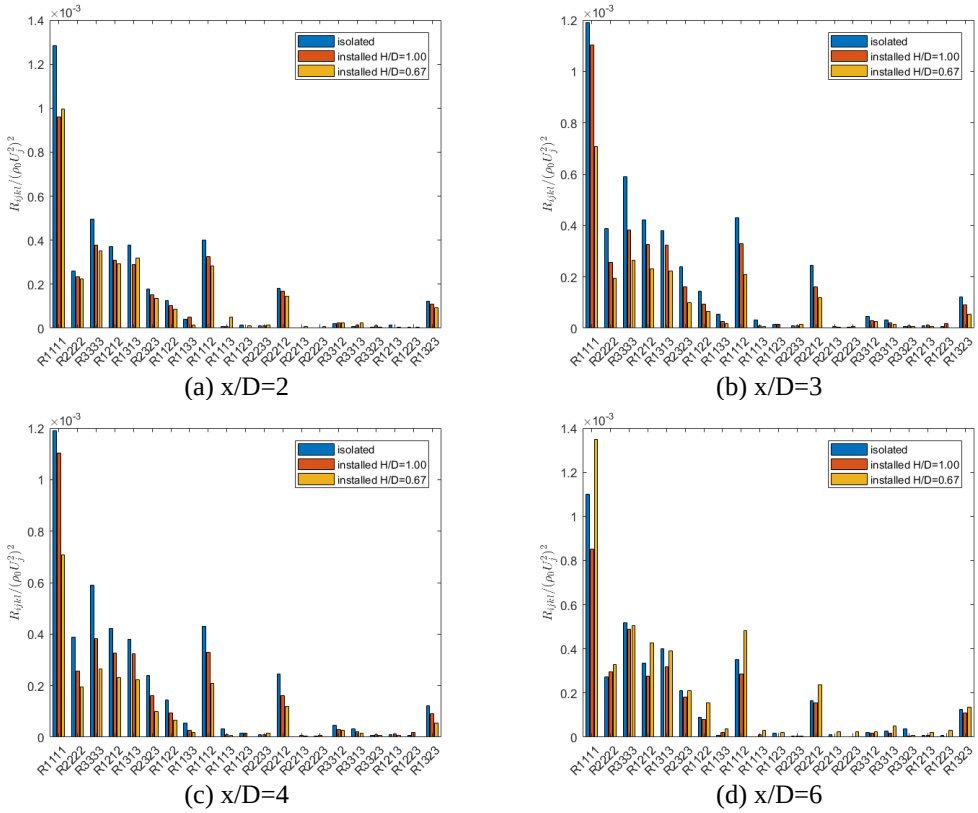
Figure 6 Normalised 4th order space-time correlation of axial velocity $R_{1111}(x;\delta x=(\delta x_1,0,0),\tau)/R_{1111}(x;\delta x=0,\tau=0)$ along the nozzle lipline y/D=0.5 at x/D=2, 3, 4, 5 and 6 for isolated and installed jets



(a) Length scales (b) Time scales (c) Convection velocity

Figure 7 Length and time scales of space-time correlations $R_{1111}(x;\delta x,\tau)$ in the moving frame with a local convection velocity

Figure 8 shows the amplitude of each quadrupole source component, $R_{ijkl}(\boldsymbol{x};\mathbf{0},0)$, at a few typical axial locations. They are under the plate (*x*/*D*=2 and 3), at the plate trailing edge (x/D=4) and downstream of the trailing edge (*x*/*D*=5). Among those components, the 4th order axial velocity correlation, R_{1111}, is the dominant source, which was used to calculate the length and time scale in Figure 7. In addition, other components, such as $R_{2222}, R_{3333}, R_{1212}, R_{1313}, R_{2323}, R_{1122}, R_{1112}, R_{2212}$ and R_{1323}, also contribute to mixing noise generation, but less significantly than R_{1111}. For installed jets, the amplitude of all the quadrupole sources is reduced by the acceleration of the flow under the plate. At *x*/*D*=2, the two installed jets, *H*/*D*=1.00 and *H*/*D*=0.67, show a similar level of quadrupole sources as both of the jet development is not restricted by the plate. At *x*/*D*=3 and 4, the jet flow has already reached the plate underneath for *H*/*D*=0.67, and a small fraction of the boundary layer starts to grow under the plate. All the quadruple source components are reduced by the plate for *H*/*D*=0.67. Further downstream of the plate, at *x*/*D*=6, all the other quadrupole components of the two installed jets have already recovered to a similar level to that of the isolated jet, except for R_{1111}. R_{1111} of the two installed jets shows a different trend compared with that of the isolated jet.

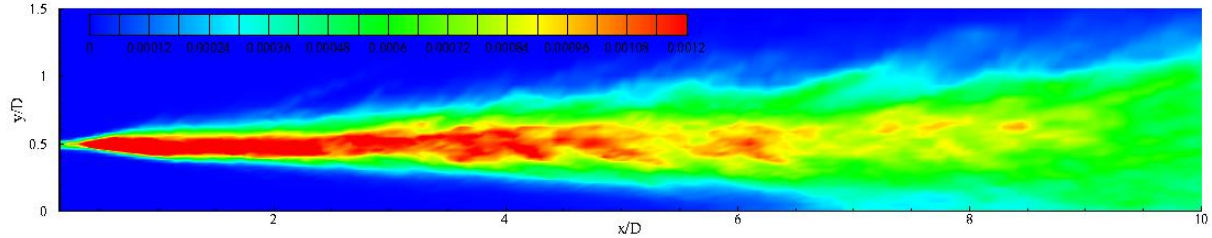


(a) x/D=2 (b) x/D=3

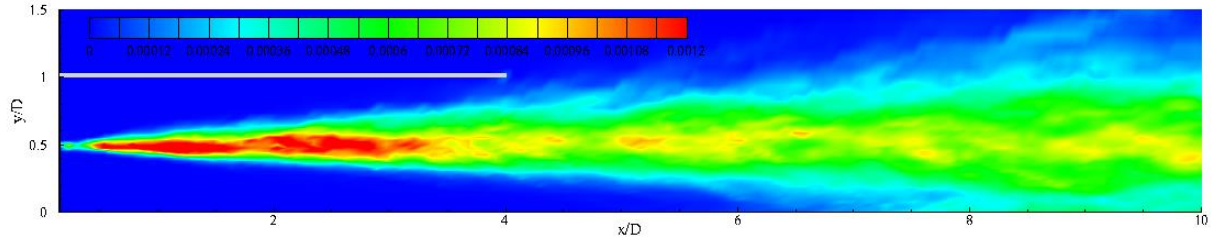
(c) x/D=4 (d) x/D=6

Figure 8 Amplitude breakdown of 4th order velocity correlation at x/D=2, 3, 4 and 6 along the lipline.

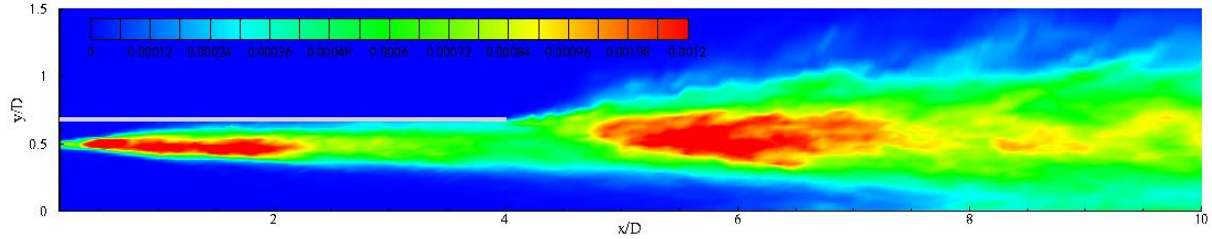
Figure 9 shows the amplitude of the dominant quadrupole source for the three jets. Compared with the isolated jets, the streamwise growth of R_{1111} is suppressed by the presence of the plate. This could be the consequence of flow acceleration beneath the plate, which leads to a decay of turbulent fluctuations. The closely installed jet H/D=067 shows a much lower level of R_{1111} after x/D as the jet shear layer scratches the plate underneath and accelerates more because of the blockage of boundary layers on the plate underneath. Directly downstream of the plate trailing edge, the R_{1111} of the installed jet H/D=1.00 is still a bit lower than that of the isolated jet but tends to return to a similar level at the further downstream locations. The closely installed jet H/D=0.67 shows a different trend. The R_{1111} shows a significant increase directly downstream of the plate until x/D~7.5. This is due to the strong interactions between the jet and the plate. These increased quadrupole sources in the installed jet H/D=0.67 could potentially contribute to the noise amplification at the high frequencies (St>1), which is observed in Figure 5 at high polar angles. This needs to be confirmed in the future by predicting far-field noise using the quadrupole sources informed by the LES data.



(a) isolated jet



(b) installed jet, H/D=1.0

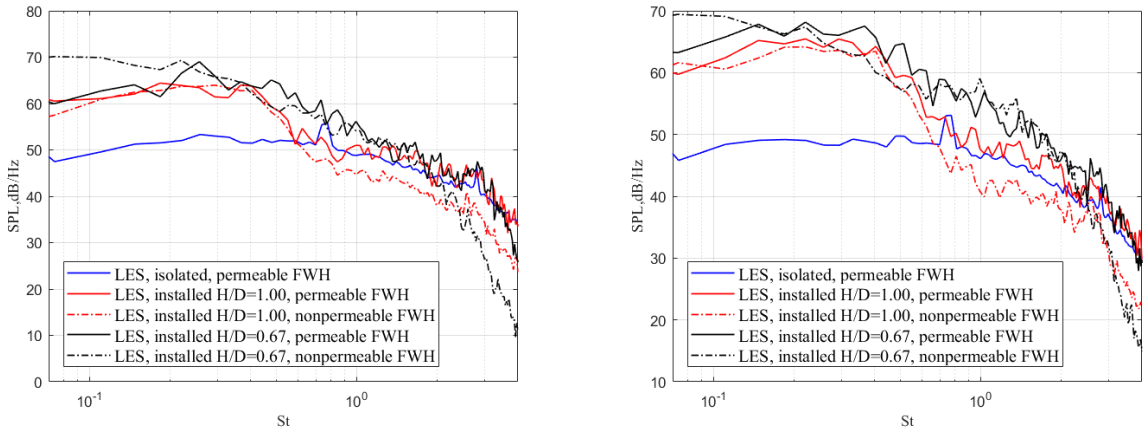


(c) installed jet, H/D=0.65

Figure 9 Amplitude of 4th order velocity correlation $R_{1111}(x;\delta x=0,\tau=0)$ for isolated and installed jets

2. Dipole sources on the plate

In addition to the noise generated by the quadrupole in the jet plume, the jet-plate interaction introduces the unsteady loadings on the plate, leading to dipole sources. The monopole is absent on this stationary solid surface. The contribution of the dipole sources to far-field noise can be evaluated by performing FW-H integration on the plate surface. Figure 10 compares the far-field noise predictions using the FW-H method on permeable surfaces around the jet and nonpermeable surfaces on the plate. The comparisons are made at two high polar angles, i.e. 90° and 120°, where the installation noise is more pronounced. Compared with the permeable FW-H prediction of the installed jets and the isolated jet, the dipole sources on the plate contribute exactly to the installation noise amplification at low frequencies (St<1). As the plate moves close to the jet, the stronger jet-plate interaction moves the noise amplification to relatively high frequencies (1<St<2) at the polar angle of 120°. This indicates that the noise amplification is primarily caused by the unsteady loading of the plate due to the jet-plate interactions.



(a) 90° polar angle (b) 120° polar angle

Figure 10 Comparison of far-field noise prediction from permeable FW-H surface around the jet and nonpermeable FW-H surface on the plate at 90° and 120° polar angles

V. Conclusion

Large-eddy simulation has been performed to investigate the closely coupled jet and surface interaction and its generated noise. It includes two installation configurations, H/D=0.67 and 1.00 for L/D=4, and one isolated jet. In the

closely-installed jet configuration H/D=0.67, the jet spreading is significantly restricted by the presence of the plate, leading to acceleration and reduction of TKE under the plate. The far-field noise predicted using the FW-H method shows that the close installation increases the noise towards relative high frequencies (1<St<2) at upstream polar angles. The noise sources can be broken down into: 1) quadrupole sources due to turbulent mixing in the jet plume and 2) dipole sources due to the unsteady loading on the plate. The quadrupole sources can be characterised by the 4th order correlation. The amplitude of leading correlation R_{1111} is amplified directly downstream of the plate in the close installation configuration H/D=0.67 while the length and time scales are also increased. This could contribute to the noise amplification in the high frequencies (St>1). Meanwhile, the far-field noise contribution of dipole sources is evaluated by performing FW-H integration on the plate surface. It shows that the unsteady plate surface loadings are the primary sources of installation noise amplification for both installed jets. It can also reproduce the relative high-frequency noise amplification (1<St<2) at upstream polar angles for the close installation configuration H/D=0.67.

In the future, the far-field noise contributed by the amplified quadrupole noise sources will be evaluated by integrating the LES-informed space-time correlations with a free-field Green's function. It also needs to confirm whether the dipole source by the strong jet-plane interaction is equivalent to the scattering of instability hydrodynamic waves at the trailing edge.

Acknowledgements

The ARCHER computing time is provided by the UK Turbulence Consortium under EPSRC grant EP/L000261/1 and PRACE Distributed European Computing Initiative.

References

1. Pepper, C.B., M.A. Nascarella, and R.J. Kendall, *A Review of the Effects of Aircraft Noise on Wildlife and Humans, Current Control Mechanisms, and the Need for Further Study.* Environmental Management, 2003. **32**(4): p. 418-432.
2. Bushell, K., *Measurement and prediction of jet noise in the fight.* AIAA aeroacoustics conference, 1975: p. AIAA 75-461.
3. Fisher, M., M. Harper-Bourne, and S. Glegg, *Jet engine noise source location: The polar correlation technique.* Journal of Sound and Vibration, 1977. **51**(1): p. 23-54.
4. Head, R.a.F., M., *Jet/surface interaction noise - analysis of far-field low frequency augmentations of jet noise due to the presence of a solid shield.* AIAA aeroacoustics conference, 1976: p. AIAA 76-502.
5. Mead, C.J. and P. Strange, *Under-wing installation effects on jet noise at the sideline.* ROLLS ROYCE PLC-REPORT-PNR, 1999.
6. Williams, J.E.F. and L.H. Hall, *Aerodynamic sound generation by turbulent flow in the vicinity of a scattering half-plane.* Journal of Fluid Mechanics, 1970. **40**(4): p. 657-670.
7. Lyu, B., A.P. Dowling, and I. Naqavi, *Prediction of installed jet noise.* Journal of Fluid Mechanics, 2017. **811**: p. 234-268.
8. Amiet, R.K., *Acoustic radiation from an airfoil in a turbulent stream.* Journal of Sound and Vibration, 1975. **41**(4): p. 407-420.
9. Pastouchenko, N. and C. Tam. *Installation Effects on the Flow and Noise of an Under-the-Wing Mounted Dual Stream Jet*. in *43rd AIAA Aerospace Sciences Meeting and Exhibit*. 2005.
10. Proença, A., J. Lawrence, and R. Self, *Investigation into the turbulence statistics of installed jets using hot-wire anemometry.* Experiments in Fluids, 2020. **61**(10): p. 1-19.
11. Jameson, A., *Formulation of kinetic energy preserving conservative schemes for gas dynamics and direct numerical simulation of one-dimensional viscous compressible flow in a shock tube using entropy and kinetic energy preserving schemes.* Journal of Scientific Computing, 2008. **34**(2): p. 188-208.
12. Wang, Z.-N., J. Tyacke, and P.G. Tucker, *Hybrid LES/RANS predictions of flows and acoustics from an ultra-high-bypass-ratio serrated nozzle.* Note on Numerical Fluid Mechanics and Multidisciplinary Design: Progress in Hybrid RANS-LES Modeling, 2018: p. 465-478.
13. Tyacke, J., Z.-N. Wang, and P. Tucker, *LES-RANS of installed ultra-high bypass-ratio coaxial jet aeroacoustics with a finite span wing-flap geometry and flight stream - Part 1: round nozzle.* AIAA paper, 2017. **2017-3854**.
14. Spalart, P.R. and S.R. Allmaras, *A one-equation turbulence model for aerodynamic flows.* Recherche Aerospatiale, 1994. **1**: p. 5-21.
15. Nicoud, F. and F. Ducros, *Subgrid-scale stress modelling based on the square of the velocity gradient tensor.* Flow, Turbulence and Combustion, 1999. **62**(3): p. 183-200.
16. Wang, Z.-N., et al., *Large-eddy-simulation prediction of an installed jet flow and noise with experimental validation.* AIAA Journal, 2020. **58**(6): p. 2494-2503.
17. Karabasov, S.A., et al., *Jet Noise: Acoustic Analogy informed by Large Eddy Simulation.* AIAA Journal, 2010. **48**(7): p. 1312-1325.
18. Goldstein, M.E., *A generalized acoustic analogy.* Journal of Fluid Mechanics, 2003. **488**: p. 18.



https://dspace.org/

LES study of noise and its sources of closely installed jets

Wang, Zhong-Nan; Proenca, Anderson R.; Lawrence, Jack; Tucker, Paul; Self, Rod

2022-06-13
American Institute of Aeronautics and Astronautics (AIAA)
https://doi.org/10.2514/6.2022-2909
Wang Z-N, Proenca A, Lawrence J, Tucker PG. (2022) LES study of noise and its sources of closely installed jets. In: 28th AIAA/CEAS Aeroacoustics 2022 Conference, 14-17 June 2022, Southampton UK, Paper number AIAA 2022-2909

Downloaded from a DSpace repository. https://dspace.org/